Spacebased observations of the seasonal changes of south Asian monsoons and oceanic responses

W. Timothy Liu and Xiaosu Xie

Jet Propulsion Laboratory, California Institute of Technology, Pasadena, CA

Abstract. The seasonal changes of **monsoons** in the South China Sea and the Arabian Sea are compared, using observations by spaceborne microwave **scatterometers** and **radiometers**. The oceanic responses to the forcing of wind stress and latent heat flux resulting from the monsoon changes are identified through **surface temperature** tendency and **sea level changes**.

remote sensing

1. Introduction

The tropical oceans between Africa and the Philippines are under the influence of monsoons. A large percentage of the world's population and their agrarian economy must endure the vagaries of these monsoons. Monsoons are the seasonal changes of wind forced by continent-ocean temperature contrasts. Besides bringing rain to land, monsoons also change ocean currents, ocean upwelling, and coastal ecology. Over land the consequences of monsoon are, perhaps, well observed, but the oceanic responses have not been sufficiently monitored.

Recently, measurements in South China Sea (SCS), which is under the influence of East Asian Monsoon System, were analyzed by Soong et al. [1995], Chu et al. [1997], and others. Before these studies, the only comprehensive survey which is accessible to the scientific community dated back almost four decades [Wyrtki, 1961]. Inferences on ocean circulation mainly came from numerical model simulation [e.g., Shaw and Chao, 1994]. The recently conducted South China Sea Monsoon Experiment [Lau, 1997] is aimed at remedying this deficiency. The Arabian Sea (AS), which is under the influence of the Indian Monsoon System, has been slightly better surveyed [e.g., Molinari et al., 1990], particularly the coastal and equatorial currents, but ocean observations are still very sparse.

Data from spaceborne microwave scatterometers and radiometers have been used to estimate the two major atmospheric forcing terms, momentum flux and latent heat flux (LHF). Spaceborne sensors also observed the surface signatures of the oceanic response: sea surface temperature (SST) and sea level changes (SLC). Although other factors also affect SST and SLC, they do not change with the monsoon winds as the two forcing terms. This report describes the initial part of the study on the monsoon forcing and response-the annual variation, using recently available spacebased data.

2. Data

The scatterometers on the European Spacecraft ERS-1 and ERS-2 have continued to make measurements of wind speed and direction under both clear and cloudy conditions since 1991. The National Aeronautics and Space Administration Scatterometer (NSCAT) was launched in August 1996 and provided 9 months of data with improved spatial resolution and coverage, before its demise in June 1997. The wind speeds and directions used in this study are derived from the three scatterometers and are interpolated to 0.5° latitude by 0.5° longitude and half-daily grid through a successive correction method [Tang and Liu, 1996; Liu et al., 1998]. The accuracy of the wind measurements may be degraded in heavy rain. The Topex/Poseidon altimeter [Fu et al., 1994] has measured SLC along ten-day repeated ground-tracks since 1992. The data are interpolated to an uniformly gridded field of 1° and 3 day resolutions, after the four-year along-track means were removed. In the shallow water of the coastal regions, SLC may be contaminated by tidal aliasing. The operational Advanced Very High Resolution Radiometers (AVHRR) are providing measurements of SST. In this study, the 1° and 7-day composite SST fields compiled by blending AVHRR data with in situ measurements [Reynolds and Smith, 1994] are used. The operational Special Sensor Microwave/Imagers (SSM/I) have monitored wind speed, integrated water vapor (IWV) since July 1987. Daily and 0.25° IWV compiled by Wentz [1996] is used in this study. The 1° and monthly LHF is computed from the wind speed and IWV from SSM/I and the SST [Liu et al., 1994].

3. Seasonal changes

For clarity, only three years of data (1992-1994) are plotted in Fig.1 to illustrate the annual variation and the interannual changes. NSCAT wind speed and direction of a recent period are added for comparison. The differences in the seasonal monsoon changes between the SCS and the AS are obvious. The onset of the winter monsoon is clear in the SCS, with a sharp increase in wind speed in September, and with steady wind direction from the northeast. The winter monsoon is much weaker in the AS. The onset of the summer AS monsoon is marked by a sharp increase in wind speed, while the summer SCS monsoon is relatively weak, with large fluctuations in wind direction due to intraseasonal activities. IWV increases sharply in May in the SCS and in June in AS, suggesting that the summer monsoon starts earlier in SCS. The year-to-year variation is quite large.

As shown by the averaged annual cycle in Fig. 2, the IWV in the SCS jumps abruptly in early May across the whole basin, but it increases from south to north in the AS starting in late April in the equatorial region and reaching the north in June. In fall, the IWV decreases from north to south in both basins. The air over the AS is dryer than that in the SCS throughout the year. In the SCS, the winds change direction

in early May, signifying the onset of the summer monsoon, at nearly the same time across the whole basin. The wind direction reverses, starting from the north in September and reaching the equatorial region in November. The large jump in strength of the winter monsoon occurs in early October. In the AS, the southwest monsoon increases in strength abruptly (onset of summer monsoon) across the whole basin in early June although the change in direction occurs earlier in the north. The demise of the summer monsoon occurs across the whole basin in September; the winter monsoon in the AS is much weaker.

4. Thermal responses

Negative correlations between LHF and sea surface temperature tendency ($\partial T/\partial t$) cover most area in both the SCS and the AS (Fig. 3), implying that change of SST is related to evaporative cooling. The correlations are computed from 132 pairs of monthly data, starting in July 1987. In the northern part of the SCS, along the coast of South China and North Vietnam, the annual cycle dominates, and the correlation is highly negative (greater than 0.8). In this region, LHF is highly positive and $\partial T/\partial t$ is highly negative in Fall, after the onset of the winter monsoon, with higher wind speed and dryer air (Fig. 1 and 2). In spring, LHF is low, and $\partial T/\partial t$ is positive.

Although the correlations are also negative over the AS and the southern part of the SCS, the magnitudes do not reach the same high level as in the northern SCS. LHF and $\partial T/\partial t$ have a semi-annual period in these regions. In the AS, the strength of the winter monsoon is weaker than the summer monsoon, but the winter air is much dryer and induces strong LHF (Fig. 2). The magnitude of LHF has two peaks in summer and winter corresponding to positive $\partial T/\partial t$, and two low values in spring and autumn, corresponding to negative $\partial T/\partial t$.

Strong positive correlations between LHF and SST are found near the coast of Somalia and Oman (not shown). The along-shore summer monsoon causes off-shore Ekman transport and coastal upwelling in the ocean. The low SST caused the low LHF along the coast. The summer monsoon off the Vietnamese coast should have a similar effect, but it is relatively weak, and the effect of coastal upwelling on LHF is not obvious.

5. Dynamic responses

Significant negative correlations between the curl of wind stress (CWS) and SLC, with the CWS leading by a month, are found in the central part of the SCS and the AS (Fig.4). The correlations are computed from 60 pairs of monthly data, starting in October 1992 for SLC. The negative correlation is

consistent with a simple Ekman pumping scenario. Cyclonic winds drive surface divergence and upwelling in the ocean; the rise of the thermocline causes lower sea levels. Anticyclonic winds cause higher SLC. The exceptions (positive correlations) are found in the coastal regions in the north and the south of SCS, off the west coast of India between 5°N and 10°N, and along the coast of Somalia.

In November, positive CWSs are clearly observed in the deep regions of the SCS (Fig. 5a) with a stronger center west of Luzon and a weaker center east of Vietnam. Strong negative CWSs prevail along the Chinese coast. One month later, in December, negative SLCs are observed stretching from Luzon to Vietnam, and positive SLCs are found in the north along the Chinese coast, and in the south along the northern coast of Borneo. The SLCs lead to two cyclonic gyres of geostrophic current (Fig. 6a), one east of Luzon and the other off the southern tips of Vietnam. Geostrophic currents are deviations from the 4-year means, computed from the gradient of SLC. In June, the weak summer monsoon causes negative CWSs in deep basins of SCS (Fig. 5b), where positive SLCs and anticyclonic geostrophic currents are also found (Fig. 6b).

In the AS, the winter monsoon is weak and positive CWSs are found between the equator and 15°N in November (Fig. 5c). Negative SLCs cover almost the entire central basin except for the area off the western coast of India. Between 5°N and 10°N, a cyclonic gyre of geostrophic current covers the western/central basin, but an anticyclonic gyre is found in the east. The strong summer monsoon causes strong positive CWSs along the coast of Oman with off-shore Ekman transport and coastal upwelling as discussed in Section 4. Strong negative CWSs are found in the deep ocean (Fig. 5d). The entire central basin is covered by positive SLCs, except for the region off the western coast of India. The SLCs west of the southern tip of India are not likely to be caused by local winds; their formation and maintenance require further study.

Send copy to TRAC

6. Discussion

Six and eleven years of respective spacebased observations by microwave scatterometers and radiometers reveal the annual variabilities of monsoons in the SCS and AS. The winter monsoon is found to be much stronger than the summer monsoon in the SCS, but the reverse is true in the AS. The summer monsoon starts earlier in the SCS than in AS, in agreement with Tao and Chen [1987]. The definition of monsoon onset varies, however, and there are large interannual variations to be examined in the next study.

LHF depends on wind speed and the vertical humidity gradient near the surface, and, therefore, changes with the monsoons. Over most of the AS and the SCS, the negative correlation between LHF and $\partial T/\partial t$ is consistent with the notion that evaporative cooling is a significant factor in the annual variations of SST, and in agreement with the results of Liu et al. [1994] over global oceans. Except in the northern part of the SCS, where an annual cycle dominated by winter monsoon is found, the variations in both ocean basins are largely semi-annual, with high LHF and evaporative cooling during both winter and summer monsoons, and low

LHF in between. Strong off-shore Ekman transport and coastal upwelling are inferred from the along-shore wind, cold SST, and low LHF off the coast of Somalia and Oman during summer, but similar upwelling off the Vietnam coast is weaker.

Significant negative correlation between CWS and SLC in the central part of the basins is consistent with seasonal changes of Ekman pumping following the monsoons. In the deep basin, positive stress curl causes upwelling, lower sea level, and anticyclonic geostrophic current in winter, and negative stress curl causes higher sea level and cyclonic geostrophic current in summer.

Acknowledgments. This study was performed at the Jet Propulsion Laboratory, California Institute of Technology, under contract with the National Aeronautics and Space Administration (NASA). It was jointly supported by the NASA Scatterometer (NSCAT), the Earth Observing System (EOS) Interdisciplinary Sciences, and the Physical Oceanography Program of NASA. Dr. Wenqing Tang assisted in the early stage of the data analysis.

References

Chu, P. C., S. Lu, and Y. Chen, Temporal and spatial variabilities of the South China Sea surface temperature anomaly, J. Geophys. Res., 102, 20,937-20,955, 1997.

Fu, L. L., E. J. Christensen, C. A. Yamarone, M. Lefebvre, Y. Menard, M. Dorrer, and P. Escudier, TOPEX/POSEIDON Mission Overview, J. Geophys. Res., 99, 24,369-24,381, 1994.

Lau, K. M., The South China Sea Monsoon Experiment (SCSMEX), Eos Trans. of Amer. Geophys. Union, 78, 599 & 603, 1997.

Liu, W. T., A. Zheng, and J. Bishop, Evaporation and solar irradiance as regulators of the seasonal and interannual variabilities of sea surface temperature, J. Geophys. Res., 99, 12623-12637, 1994.

Liu, W. T., W. Tang, and P. S. Polito, NASA Scatterometer provides global ocean-surface wind fields with more structures than numerical weather prediction, Geophys. Res. Lett., 25, 761-764, 1998.

Molinari, R. L., D. Olson, G. Reverdin, Surface current distribution in the tropical Indian Ocean derived from compilations of surface buoy trajectories, J. Geophys. Res., 95, 7217-7238, 1990.

Reynolds, R. W. and T. M. Smith, Improved global sea surface temperature analyses using optimum interpolation, J. Climate, 7, 929-948, 1994.

Shaw, P. T. and S. Y. Chao, Surface circulation in the South China Sea, Deep Sea Res., 41, 1663-1683, 1994.

Soong, Y. S., J. H. Hu, C. R. Ho and P. P. Niiler, Cold core eddy detected in South China Sea, Eos Trans. of Amer. Geophys. Union, 76, 345 & 347, 1995.

Tang, W. and W. T. Liu, Objective Interpolation of Scatterometer Winds, JPL Publication 96-19, Jet Propulsion Laboratory, Pasadena, 16 pp, 1996.

Tao, S. Y. and L. X. Chen, A review of recent research on the east Asian summer monsoon in China, Monsoon Meteorology, C. P. Chang and T. N. Krishnamurti (eds.), Oxford University Press, 60-92, 1987.

Wentz, F. J., A well-calibrated ocean algorithm for special sensor microwave/imager, J. Geophys. Res., 102, 8703-8718, 1996.

Wyrtki, K., Scientific Results of Marine Investigations of the South China Sea and the Gulf of Thailand 1959-1961, NAGA Report Vol 2, Univ. of Calif. Scripps Institution of Oceanography, 193 pp., 1961.

W. T. Liu and Xiaosu Xie, Jet Propulsion Laboratory, California Institute of Technology, 4800 Oak Grove Drive, MS 300-323, Pasadena, CA 91109. (e-mail: liu@pacific.jpl.nasa.gov)

(Received January 22, 1998; revised March 12, 1999;
accepted March 25, 1999.)

Captions

Fig. 1 Time series of (from top to bottom) wind speed, wind direction, and integrated water vapor at (a) 19°N and 115°E in the South China Sea, and (b) 19°N and 70°E in the Arabian Sea.

Fig. 2 Time-latitude section of the climatological-average of water vapor, zonal component, and meridional component of surface winds along (a) 115°E, and (b) 65°E.

Fig. 3 Distribution of correlation coefficients between the latent heat flux and the sea surface temperature tendency in (a) SCS, and (b) AS.

Fig. 4 Correlation Coefficients between curl of wind stress and sea level changes, with curl of wind stress leading sea level changes by 1 month, in (a) SCS, and (b) AS.

Fig. 5 Distribution of curl of wind stress (10⁻6N/m3) (a) in SCS for November, (b) in SCS for June, (c) in AS for November, and (d) in AS for June. The arrows are surface wind vectors.

Fig. 6 Distribution of sea level changes (m) (a) in SCS for December, (b) in SCS for July, (c) in AS for December, and (d) in AS for July. The arrows represent the geostrophic current.

Fig. 1 Time series of (from top to bottom) wind speed, wind direction, and integrated water vapor at (a) 19°N and 115°E in the South China Sea, and (b) 19°N and 70°E in the Arabian Sea.

Fig. 2 Time-latitude section of the climatological-average of water vapor, zonal component, and meridional component of surface winds along (a) 115°E, and (b) 65°E.

Fig. 3 Distribution of correlation coefficients between the latent heat flux and the sea surface temperature tendency in (a) SCS, and (b) AS.

Fig. 4 Correlation Coefficients between curl of wind stress and sea level changes, with curl of wind stress leading sea level changes by 1 month, in (a) SCS, and (b) AS.

Fig. 5 Distribution of curl of wind stress ($10^{-6}N/m^3$) (a) in SCS for November, (b) in SCS for June, (c) in AS for November, and (d) in AS for June. The arrows are surface wind vectors.

Fig. 6 Distribution of sea level changes (m) (a) in SCS for December, (b) in SCS for July, (c) in AS for December, and (d) in AS for July. The arrows represent the geostrophic current.

LIU AND XIE: SPACEBASED OBSERVATIONS OF THE SEASONAL CHANGES

LIU AND XIE: SPACEBASED OBSERVATIONS OF THE SEASONAL CHANGES

Fig 1

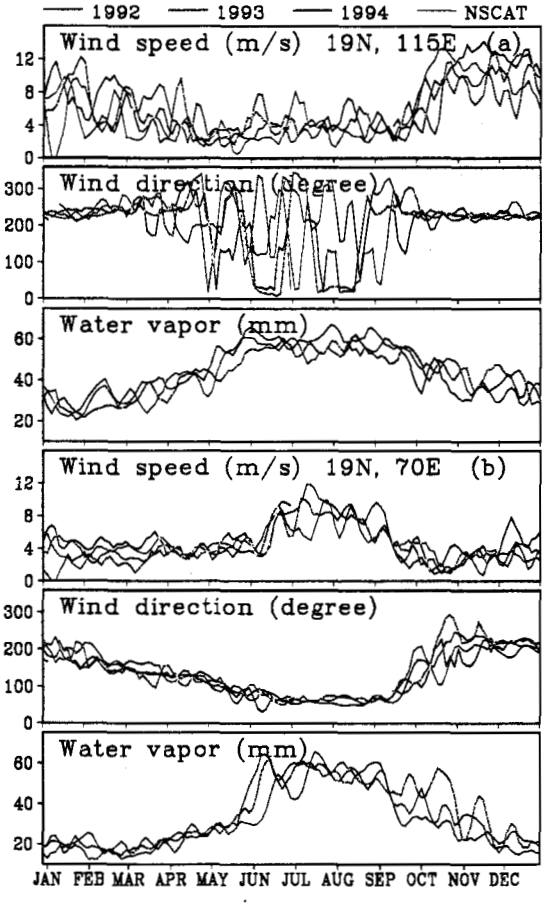
1992
1993
1994
NSCAT
Wind speed (m/s) 19N, 115E (a)
12
8
4
0
Wind direction (degree)
300
200
100
0
Water vapor (mm)
60
40
20
Wind speed (m/s) 19N, 70E (b)
12
8
4
0
Wind direction (degree)
300
200
100
0
Water vapor (mm)
60
40
20
JAN FEB MAR APR MAY JUN JUL AUG SEP OCT NOV DEC

FIG 2

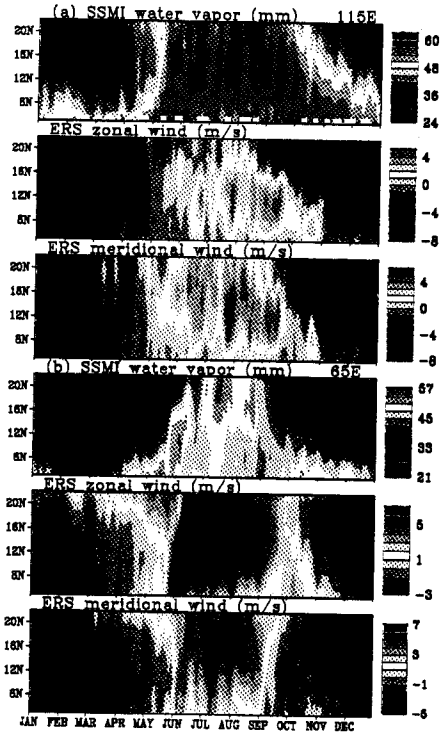
(a) SSMI water vapor (mm) 115E
20N
16N
12N
8N
60
48
36
24
ERS zonal wind (m/s)
4
0
-4
-8
ERS meridional wind (m/s)
4
0
-4
-8
(b) SSMI water vapor (mm) 65E
57
45
33
21
ERS zonal wind (m/s)
5
1
-3
ERS meridional wind (m/s)
7
3
-1
-5
JAN FEB MAR APR MAY JUN JUL AUG SEP OCT NOV DEC

Fig 3

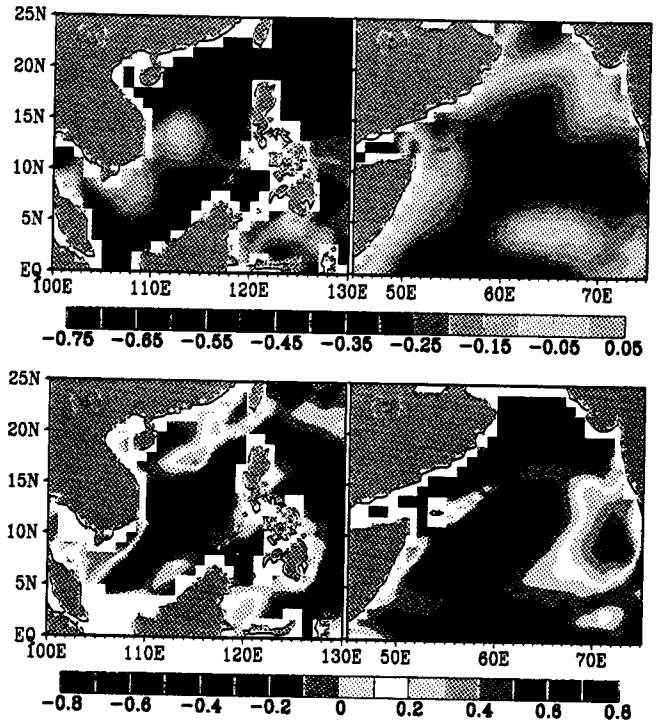
25N
20N
15N
10N
5N
EQ
100E
110E
120E
130E
50E
60E
70E
−0.75 −0.65 −0.55 −0.45 −0.35 −0.25 −0.15 −0.05 0.05
25N
20N
15N
10N
5N
EQ
100E
110E
120E
130E
50E
60E
70E
−0.8 −0.6 −0.4 −0.2 0 0.2 0.4 0.6 0.8

Fig. 4

Fig 5

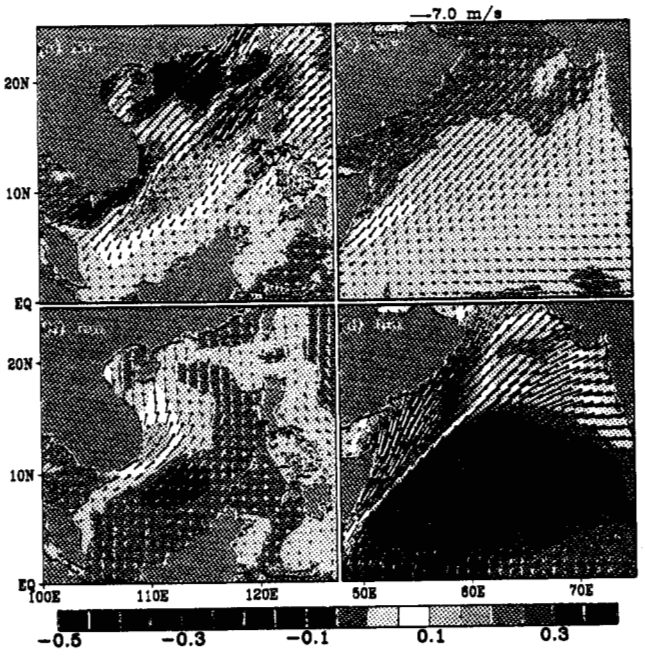
7.0 m/s
20N
10N
EQ
20N
10N
EQ
100E
110E
120E
50E
60E
70E
−0.5
−0.3
−0.1
0.1
0.3

Fig 5

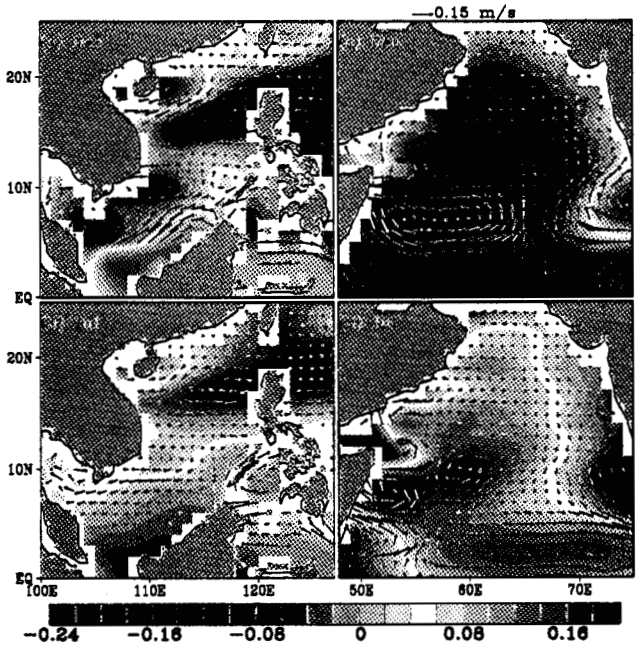
—0.15 m/s
20N
10N
EQ
20N
10N
EQ
100E
110E
120E
50E
60E
70E
−0.24
−0.16
−0.08
0
0.08
0.16